

# The census of nuclear activity of late-type galaxies in the Virgo cluster

R. Decarli,<sup>1,2\*</sup> G. Gavazzi,<sup>1</sup> I. Arosio,<sup>1</sup> L. Cortese,<sup>3</sup> A. Boselli,<sup>4</sup> C. Bonfanti,<sup>1</sup> M. Colpi<sup>1</sup>

<sup>1</sup> *Università degli Studi di Milano-Bicocca, Piazza delle scienze 3, 20126 Milano, Italy*

<sup>2</sup> *Università degli Studi dell'Insubria, via Valleggio 11, 22100 Como, Italy*

<sup>3</sup> *School of Physics and Astronomy, Cardiff University, The Parade, Cardiff CF24 3YB*

<sup>4</sup> *Laboratoire d'Astrophysique de Marseille, BP8, Traverse du Siphon, F-13376 Marseille, France*

9 August 2021

## ABSTRACT

The first spectroscopic census of AGNs associated to late-type galaxies in the Virgo cluster is carried on by observing 213 out of a complete set of 237 galaxies more massive than  $M_{\text{dyn}} > 10^{8.5} M_{\odot}$ . Among them, 77 are classified as AGNs (including 21 transition objects, 47 LINERs and 9 Seyferts), and comprize 32 % of the late-type galaxies in Virgo. Due to spectroscopic incompleteness at most 21 AGNs are missed in the survey, so that the fraction would increase up to 41 %. Using corollary Near-IR observations, that enable us to estimate galaxies dynamical masses, it is found that AGNs are hosted exclusively in massive galaxies, i.e.  $M_{\text{dyn}} \gtrsim 10^{10} M_{\odot}$ . Their frequency increases steeply with the dynamical mass from zero at  $M_{\text{dyn}} \approx 10^{9.5} M_{\odot}$  to virtually 1 at  $M_{\text{dyn}} > 10^{11.5} M_{\odot}$ . These frequencies are consistent with the ones of low luminosity AGNs found in the general field by the SDSS. Massive galaxies that harbor AGNs commonly show conspicuous  $r$ -band star-like nuclear enhancements. Conversely they often, but not necessarily contain massive bulges. Few well known AGNs (e.g. M61, M100, NGC4535) are found in massive Sc galaxies with little or no bulge. The AGN fraction seems to be only marginally sensitive to galaxy environment. We infer the black hole masses using the known scaling relations of quiescent black holes. No black holes lighter than  $\sim 10^6 M_{\odot}$  are found active in our sample.

**Key words:** galaxies: nuclei – galaxies: clusters: individual (Virgo)

## 1 INTRODUCTION

Active Galactic Nuclei (AGNs) can be broadly divided in classes of decreasing luminosity from quasars, Seyfert to Low-Ionization Nuclear Emission Regions (LINERs) characterized by narrow emission lines of relatively low ionization and large [NII]/H $\alpha$  line ratios. A growing body of evidences, triggered by studies of low luminosity AGNs, from radio to X-rays (Halderson et al. 2001, Terashima et al. 2002, Filho et al. 2004, Martini et al. 2006) and in particular in the optical band, mostly owing to the Sloan Digital Sky Survey (SDSS; York et al. 2000) is reinforcing the scenario where LINERs represent the missing link between higher luminosity AGNs and dormant supermassive black holes. Hao et al. (2005) estimate that 4-10 % of all galaxies in the SDSS harbor an AGN; Kauffmann et al. (2003) estimate that up to 80% of galaxies of more than  $10^{11} M_{\odot}$  harbor a supermassive black hole, either dormant or active.

The role of the environment in triggering or inhibiting nuclear activity is still not clear. Dressler et al. (1985) observed an AGN fraction in the field  $\sim 5$  times higher than in clusters. Kauffmann et al. (2004) found that the fraction of powerful AGNs (with high [OIII] luminosity, i.e. dominated by Seyferts) in the SDSS decreases with increasing galaxy environment density. They interpret this result in connection with the fact that strong AGNs are hosted in star-forming galaxies that avoid dense environments. Popesso & Biviano (2006) found that the AGN fraction decreases with increasing velocity dispersion of galaxies in groups and clusters, being higher in dense, low-dispersion groups. On the other hand, Shen et al. (2007) suggest that the fraction of AGNs in galaxy groups and in clusters may be the same. Miller et al. (2003) find that the frequency of low activity AGNs is insensitive to the environment. Furthermore, Boselli & Gavazzi (2006) showed that gravitational interaction between the galaxy and the cluster potential as a whole does trigger gas infall toward the galaxy center, and this may feed nuclear activity.

\* roberto.decarli@mib.infn.it

The Virgo Cluster provides a perfect environment for studying the relations between the nuclear activity and the host galaxy, for at least four reasons: 1) it's near enough to grant us a highly detailed knowledge of the host galaxy internal structure and morphology; the nuclear component is also easily disentangled among inner galaxy regions; 2) a complete survey of a wide range of luminosity can be achieved; 3) many galaxies member of the Virgo Cluster have been studied individually in almost all the electromagnetic spectrum (e.g., Allard et al. 2006; Garca-Burillo, et al., 2005; Chyży et al., 2006; Boselli et al. 2006; Yoshida et al. 2004); 4) the environmental effects on the nuclear activity may be examined through various indicators (i.e. gas deficiency).

Coté et al. (2006), analyzing 100 Elliptical galaxies in the Virgo cluster surveyed with the ACS on board the HST by Ferrarese et al. (2006a), find that most (66-82 %) contain nuclear cusps, mainly in galaxies less massive than  $3 \cdot 10^{10} M_{\odot}$ . Wehner & Harris (2006) and Ferrarese et al. (2006b) found that the masses of these bright cusps follow the same scale relations as the black hole (BH) masses in giant ellipticals, occupying the same range as the lower-end extrapolation of the  $M_{\text{BH}} - \text{Magnitude}$  correlation. This suggests that a common mechanism is responsible for the growth of both nuclear stellar cusps or black holes on these mass scales.

As far as late-type galaxies in the Virgo cluster, instead, no systematic survey exists providing the census of massive BHs nor of AGNs of the various species. To fill this gap we undertook a survey of virtually all spiral galaxies brighter than 15 mag belonging to the Virgo cluster, probing their activity with diagnostic tools that are sensitive to the presence of low activity AGNs. In spite of the poorer statistics, the Virgo spirals appear to have AGN properties consistent with the ones in the SDSS, i.e. their frequency depends critically on the mass of the hosts galaxies. By exploiting the superior resolution obtained at the distance of the Virgo cluster we show that AGNs develop in large mass galaxies that have significant stellar nuclei, independently from the existence of conspicuous bulges.

## 2 SAMPLE

The present analysis is based on a volume limited, complete set of late-type galaxies belonging to the Virgo cluster. The sample is obtained by selecting from the Virgo Cluster Catalogue (Binggeli et al. 1985, 1993) all cluster members ( $-1000 < Vel < 3000$  km/s) with apparent photographic magnitude brighter than 15.0 mag and Hubble type between Sa and Im/BCD. A distance of  $D=17.0$  Mpc is assumed for all clouds constituting the Virgo cluster, except W, M ( $D=32$  Mpc) and B ( $D=23$  Mpc) (see Gavazzi et al. 1999), equivalent to assuming an Hubble constant of  $H_o = 75$  km s $^{-1}$ Mpc $^{-1}$ . The resulting sample comprises 237 galaxies brighter than  $M_{\text{pg}} \approx -16$  mag.

## 3 DATA

For the aim of the present study, for each of the target galaxies we collect three sets of observations: Near-IR (H-band) imaging, optical (Gunn  $r$ -band) imaging and intermediate resolution ( $R \sim 1000$ ) spectroscopy. These quanti-

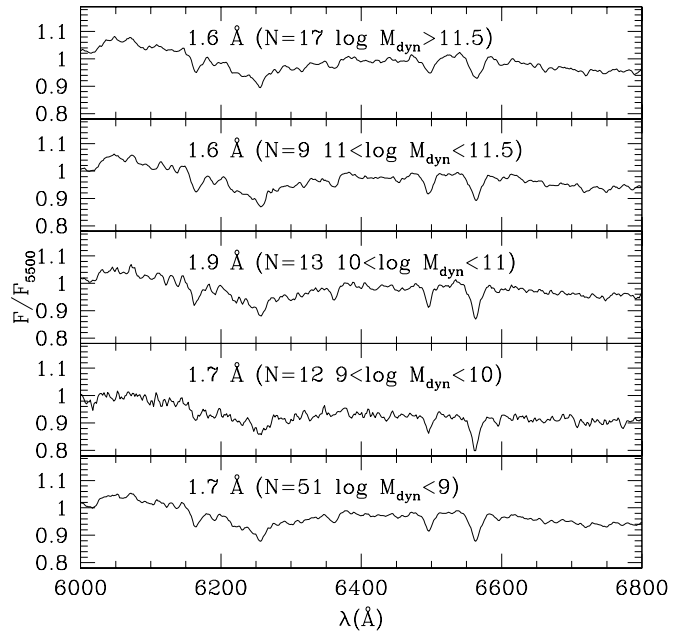


**Figure 1.** Red-channel template spectra near H $\alpha$  of early-type galaxies binned in 4 mass intervals and all together (bottom) are used to estimate the underlying continuum at H $\alpha$ . The E.W. of H $\alpha$ , the number of averaged spectra and the mass interval are labeled.

**Table 1.** Completeness.

$m_{\text{pg}} \leq 15.0$	Near-IR	$r$ -band	Spec.classif.
237	216	199	213

ties are partly derived from existing observations available from the WEB site GOLDMine (Gavazzi et al. 2003), partly obtained on purpose for the present investigation. Table 1 gives the coverage of the various data sets, stressing the high degree of completeness of the spectral classification (213/237=90%), of the optical (199/237=84%) and Near-IR imaging (216/237=91%). Near-IR imaging was obtained as described in Gavazzi et al. (2001) (and references therein) and from 2MASS. H-band total luminosities ( $L_H$  in  $L_{\odot}$ ) are obtained from extrapolation to infinity of light profiles fitted to isophotal ellipses (Gavazzi et al. 2000). For 21 galaxies without Near-IR data,  $L_H$  is derived from the photographic luminosity:

$$\log L_H = 0.80 - 0.50(M_{\text{pg}}) \quad (1)$$

where  $M_{\text{pg}} = m_{\text{pg}} - 5 \log D - 25$ . Equation 1 was obtained by fitting the H-band luminosity and the  $M_{\text{pg}}$  of 440 late-type galaxies with available data in the GOLDMine database. The dispersion of this relation is in the order of 0.2 dex.

$L_H$  provides us with an estimate of the dynamical mass within the optical radius of disk galaxies (Gavazzi et al. 1996), according to  $\log M_{\text{dyn}} = \log L_H + 0.66$ . From the Near-IR images we also derive the H-band light concentration index  $C_{31}$ , i.e. the ratio of the radii containing 75 and 25 % of the total light. This parameter is sensitive to the presence of conspicuous central bulges (with  $C_{31}$  in excess

**Table 2.** Spectral available data. ‘Ho’ refers to line fluxes published in Ho, Filippenko & Sargent (1997); ‘SDSS’ to SDSS DR5 spectra; ‘Loiano’ to Loiano nuclear spectra; ‘DS’ and ‘mDS’ refer to Drift-Scan and modified Drift-Scan spectra, as described in the text; ‘NED’ lists the galaxy nuclear classification available in the NASA/IPAC Extragalactic Database.

	Ho	SDSS	Loiano	mDS	DS	NED	All
<i>Available</i>	40	84	29	22	193	41	409
<i>Adopted</i>	40	73	13	4	81	2	213

of 4-5, while pure disks have  $C_{31} \sim 2.8$  – see Gavazzi et al., 2000).

As part of the  $H\alpha$  imaging survey of Virgo spirals, complete down to  $m_{\text{pg}} \leq 16.5$  (Gavazzi et al. 2006),  $r$ (Gunn) images were obtained to estimate the red stellar continua. Here we use the 199 images available for the present sample to estimate and quantify the presence of relevant nuclear enhancements. For each galaxy we construct the parameter  $Nuc(r)$  as the difference of the  $r$ -band surface brightness within 1.5 of the seeing disk and the mean surface brightness between 25 and 50 % of the  $r$ -band radius. Galaxies with  $Nuc(r)$  in excess of 1 ( $\text{mag arcsec}^{-2}$ ) have significant optical nuclei, harboring approximately  $10^9$  years old stars, or contributed by the AGN continuum radiation<sup>1</sup>.

Our analysis is based on the ratios of narrow emission line fluxes. Different sets of spectroscopic data are used on this purpose. The first line of Table 2 lists all the available spectroscopic material, indicating that for many of the 237 sampled galaxies more than one spectroscopic source is available. The second line gives the 213 independent measurements that were finally adopted after choosing among various possibilities, according to the following priorities. We first checked their availability in Ho et al. (1997). If present we adopt the line ratios, not the final classification given in that paper. Secondly we measure the line fluxes on available nuclear spectra. 84 spectra, obtained with apertures of 3 arcsec, were published in the SDSS in the fifth data release (Adelman-McCarthy, J., et al. 2007). 73 of these lacked of a classification in Ho et al. (1997). Other nuclear spectra were obtained on purpose in February and March 2005, 2006 using the Bologna-Faint-Object-Spectrograph (BFOSC) attached to the Loiano 1.5m telescope. These consist of nuclear long-slit spectra taken through a 2-arcsec slit, combined with an intermediate-resolution grism ( $R \sim 1000$ ) covering however only a limited amount of the red-channel (6100 - 8200 Å), containing  $H\alpha$  and [NII], but not  $H\beta$  nor [OIII]. Out of the 29 spectra taken at Loiano only 13 were adopted for the final classification because we often preferred the Ho and SDSS spectra, covering a broader spectral range.<sup>2</sup> 193 spec-

tra available for galaxies in the present study were taken from the GOLDMine database. These spectra were taken in the drift-scan mode (labeled “DS” after Drift-Scan in Table 2), i.e. letting the slit of the spectrograph, parallel to the galaxy major-axis, slide across the minor-axis (Gavazzi et al. 2004). Spectra taken in this modality maintain their spatial resolution only along the slit. DS spectra typically cover the 3500-7000 Å range with  $R \sim 600 - 1000$ . Since they are usually employed to study the overall, luminosity-averaged spectral characteristics of galaxies, the aperture is kept wide enough to integrate over a large fraction of the slit. Twenty-two of the DS spectra were also re-extracted with a smaller ( $\sim 5$  arcsec) aperture. These data are labeled as “modified DS”. The role of these data is further discussed in section 4.2. Finally, the NASA/IPAC Extragalactic Database reports, without completeness, the nuclear classification of 41 objects in our sample. Only 2 of them had no other spectral data in our study, and were thus classified according to NED.

In all available spectra (excluding Ho et al. 1997) we measured the intensity of the [OIII], [NII] and the narrow-component  $H\beta$  and  $H\alpha$  emission lines. Underlying  $H\beta$  absorption is measured separately (as explained in Gavazzi et al. 2004) and the adopted value of  $H\beta$  in emission is corrected accordingly. Underlying  $H\alpha$  is not equally easy to measure for most emission-line objects. To estimate the underlying  $H\alpha$  and correct for it one could use several approaches. The most recommended one would be that of fitting stellar population synthesis models (e.g. Bruzual & Charlot, 2003) to the observed spectra and measuring  $H\alpha$  from the models. The drawback of this method is that it suffers from uncertainties in the extinction correction, unless UV and Far-IR data were available, which is not the case for nuclear regions. We therefore preferred a simpler method based on the assumption that elliptical-like objects are realistic representations of the circumnuclear stellar properties of galaxies. We therefore assembled template spectra of 51 early-type galaxies available from GOLDMine, binned in 4 mass intervals (each containing tens of spectra). It is apparent from Figure 1 that the amount of absorption at  $H\alpha$  is independent of the galaxy luminosity. We therefore combined all available early-type spectra into a unique template spectrum that we subtract (after normalization) from the individual emission line spectra. On average the E.W. of the underlying  $H\alpha$  is  $\sim 1.7$  Å. If line fluxes fell under the sensitivity limit ( $\lesssim 3\sigma$  of the rms of the spectral continuum), we classified the galaxy as No Emission Line (NEL) galaxy.

## 4 ANALYSIS

Table 5 lists the relevant photometric and spectroscopic parameters derived in this work. The content of the individual columns is listed at the end of the table.

### 4.1 AGN diagnostics

There are various semi-empirical criteria to separate normal from AGN galaxies and, within the latter, various levels of

as LINER. The spectroscopic coverage now reaches 93% of the sample.

<sup>1</sup> The nuclearity parameter was not derived from the Near-IR data-set because these images are not of sufficient seeing quality to derive a nuclear parameter, whereas they are adequate for determining  $C_{31}$

<sup>2</sup> Note added in proofs: among the 23 unobserved galaxies listed at the end of Table 5, 7 were observed with the Loiano telescope in spring 2007, leading to the following results: VCC99, 449, 567, 697, 1442, CGCG14062 (with  $\log(L_H/L_\odot) < 9.75$ ) have HII-like nuclei. The brightest VCC362 ( $\log(L_H/L_\odot) = 10.46$ ) is classified

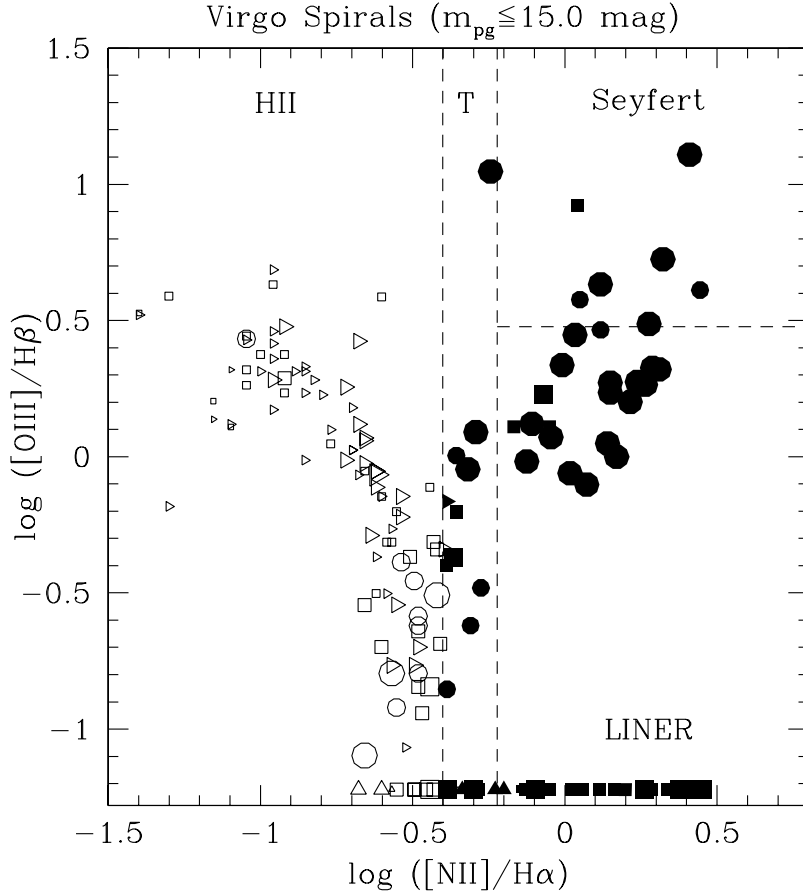


**Figure 2.** The 2-D diagnostic diagram (the BPT diagram, from Baldwin, Phillips & Terlevich, 1981) used to characterize the spectra of galaxies in this work based on the  $[\text{NII}]/\text{H}\alpha$  and  $[\text{OIII}]/\text{H}\beta$  line ratios. Objects for which  $[\text{OIII}]/\text{H}\beta$  is not available either because the spectra were taken in the red-channel (Loiano spectra) or lines were too weak to be measured, are plotted at  $\log([\text{OIII}]/\text{H}\beta) = -1.2$ . Triangles are for drift-scan spectra, squares are for the our nuclear spectra (Loiano+SDSS+modified drift-scan), while circles are from Ho et al.(1997); empty symbols are for HII-like nuclei, filled symbols for Transition, LINER and Seyfert. Symbol size is proportional to the dynamical mass.

**Table 3.** Spectral classification for all the available data. The number of adopted classification separately for each data source is reported in parenthesis.

Set	Ho	SDSS	Loiano	mDS	DS	NED	Adopted
Seyfert	7 (7)	2 (1)	0 (0)	0 (0)	1 (0)	12 (1)	9
Sey/LIN	0 (0)	15 (14)	15 (5)	18 (3)	26 (1)	3 (0)	23
LINER	17 (17)	7 (6)	0 (0)	0 (0)	0 (0)	11 (1)	24
LIN/HII	6 (6)	8 (6)	4 (3)	1 (1)	20 (5)	2 (0)	21
HII	10 (10)	44 (38)	8 (5)	2 (0)	136 (68)	13 (0)	121
NEL	0 (0)	8 (8)	2 (0)	1 (0)	10 (7)	0 (0)	15
AGN	30	32	19	19	47	28	77
All	40	84	29	22	193	41	213
$f_{\text{AGN}}$	0.75	0.38	0.66	0.86	0.24	0.68	0.36

AGN activity. They all rely on 2-D line diagnostic diagrams involving  $[\text{OIII}]_{\lambda 5007}/\text{H}\beta$ ,  $[\text{NII}]_{\lambda 6584}/\text{H}\alpha$ ,  $[\text{OI}]_{\lambda 6300}/\text{H}\alpha$  and  $([\text{SII}]_{\lambda 6717} + [\text{SII}]_{\lambda 6731})/\text{H}\alpha$  (see e.g. Baldwin, Phillips & Terlevich, 1981; Veilleux & Osterbrock 1987; Kewley et al. 2001; Kauffmann et al. 2003). The reader is referred to Stasinska et al. (2006) for a detailed comparison of these diagnostic tools. In this paper we adopt the following definitions (see Figure 2):

1) for all spectra we adopt  $[\text{NII}]/\text{H}\alpha < 0.4$  to unambiguously identify HII-like nuclei,  $0.4 < [\text{NII}]/\text{H}\alpha < 0.6$  for transition objects (HII/LIN) and  $[\text{NII}]/\text{H}\alpha > 0.6$  for AGNs.

2) if the blue spectrum is available and if  $[\text{OIII}]$  and  $\text{H}\beta$  are detected we split the AGNs among LINERs ( $[\text{OIII}]/\text{H}\beta < 3$ ) and Seyfert ( $[\text{OIII}]/\text{H}\beta \geq 3$ ), otherwise we classify them as Sey/LIN.

Table 3 summarizes the results of the adopted classifica-

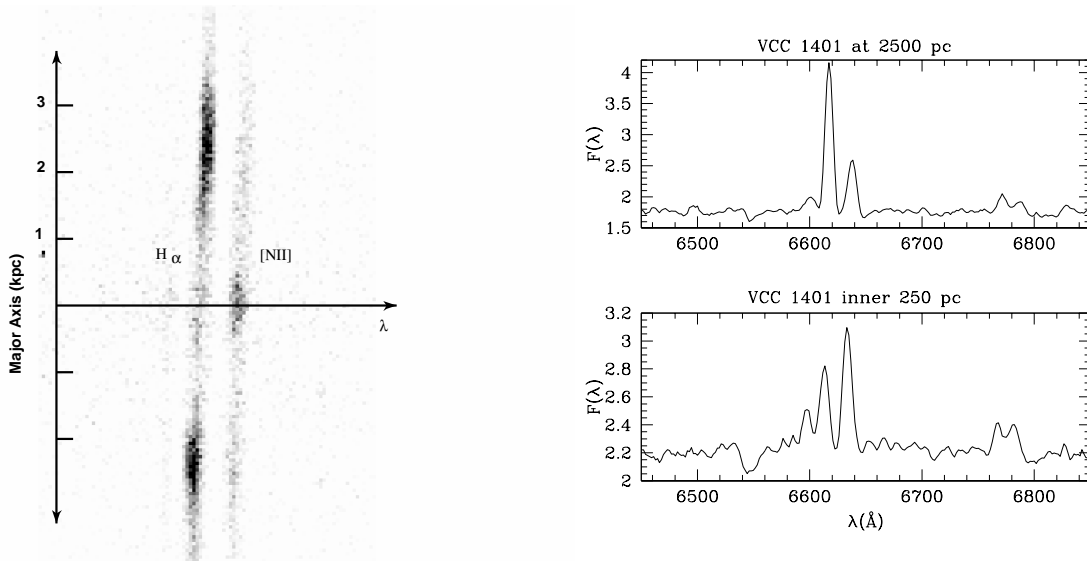


**Figure 3.** Blow-up of the 2-D long-slit Drift-Scan spectrogram of VCC1401 in the region of  $H\alpha$ , showing the inversion of the  $[NII]/H\alpha$  ratio taking place approximately at 500 pc. The nuclear spectrum in the inner 250 pc from the center of the AGN VCC1401 (bottom-right panel) and at 2.5 kpc from the center (top-right panel).

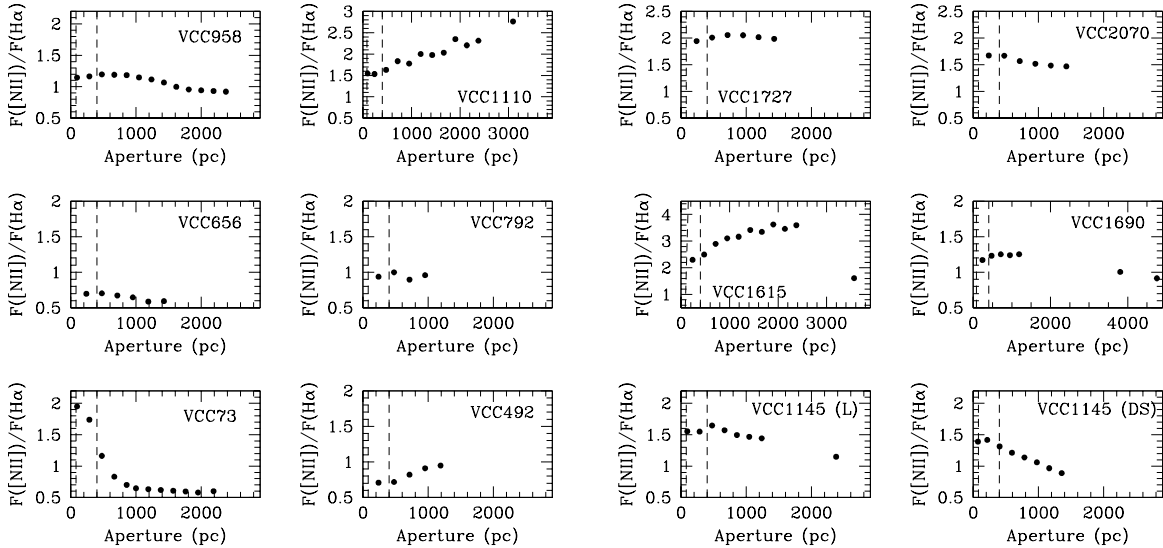


**Figure 4.** The  $[NII]/H\alpha$  ( $H\alpha$  corrected for absorption) ratio in 11 Virgo galaxies with nuclear long-slit spectra taken at Loiano is plotted as a function of the aperture in which the spectrum was extracted. The inner vertical dashed line corresponds to the seeing. The outer one gives the seeing if the galaxy was at 5 times the Virgo distance, i.e. at Coma. One galaxy (e.g. VCC 1145) is given twice: as derived from the Loiano nuclear spectrum (L) and from the Drift-scan mode spectrum (DS), the two being consistent.

tion. Data sources are listed in order of decreasing “weight” from left to right.

#### 4.2 Spatial distribution of the $[NII]/H\alpha$ ratio

Ionization conditions higher than the normal stellar contribution characterize the AGNs narrow-line region, with a spatial extent not exceeding some hundred pc (Bennert et al. 2006). A clear-cut example is the giant galaxy VCC 1401, hosting an AGN (Ho et al. 1997); our 2-dimensional DS

spectrum is shown in Figure 3 (left panel). When integrating over the inner 250 pc, the  $[NII]$  and  $H\alpha$  lines intensity ratio is typical of AGNs. On the other hand, the line emission around 2500 pc is typical of normal star-forming regions (Figure 3, right panels). This example emphasizes that DS spectra may underestimate the number of AGNs in our sample, when AGN contribution is strongly contaminated from outer HII-regions.

It was quite surprising however to find that among the 11 AGNs for which we have long slit nuclear spectra taken

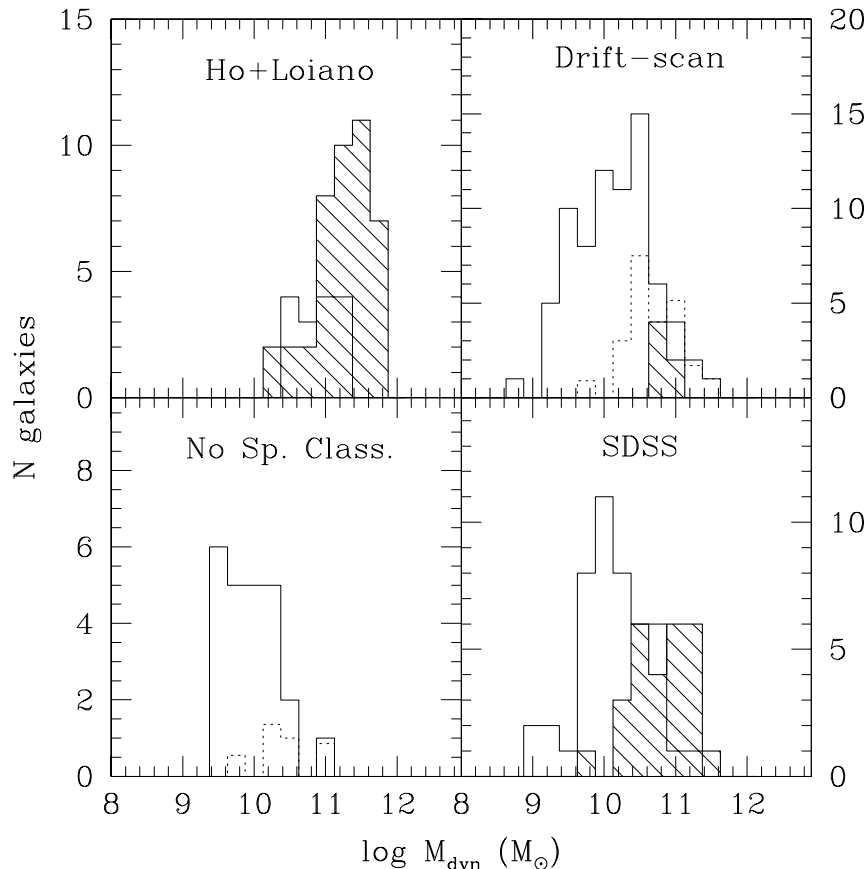


**Figure 5.** The observed distribution of AGNs (shaded) and HII region-like nuclei (thick histogram) as a function of the host galaxy dynamical mass, given separately for the Ho+Loiano spectra (top-left); for the SDSS spectra (bottom right); for the Drift-Scan spectra (top-right). The bottom-left panel shows the luminosity distribution of 24 galaxies that were not spectroscopically classified. The dashed histograms show the expected frequency of AGNs among unclassified and Drift-scan objects, extrapolated from the distribution of AGNs in the SDSS sample.

at Loiano with sufficient signal to follow the line intensity at significant distances from the nucleus (see Figure 4), in only one galaxy (i.e. VCC 73) the high ionization conditions found in the nucleus drop to HII-like within 1 kpc. In 90% of the remaining objects they prevail up to radii significantly exceeding 1 kpc. Some galaxies (e.g. VCC 1110) show an even increasing  $[\text{NII}]/\text{H}\alpha$  ratio up to 3 kpc!, in agreement with Veilleux et al. (2003) who found extended ionization conditions in NGC1365 (see their Fig 6d). Even in Drift-scan spectra these galaxies would have been recognized as AGNs, as it is the case for VCC1145, whose spectra are available in both the nuclear form (L) and Drift-scan mode (DS), showing consistency.

It is worth thus estimating the number of possibly missed AGNs because of the use of DS spectra, as illustrated in Figure 5. While the spectra obtained by Ho et al. (1997) and by us at Loiano were mostly of luminous objects, DS and SDSS spectra cover all the luminosity range of the galaxies in our sample. If the DS method would bias against AGNs, a luminosity dependence would be artificially injected. If we assume that the correct rate of AGNs as a function of mass is sampled with the nuclear spectra from

the SDSS, we expect that, among all the 193 DS spectra, 87 should have AGNs signature, that means, the DS data have a 54 % efficiency in detecting AGNs. Most of these objects lie in the narrow interval of mass ( $10^{10} - 10^{10.5} M_{\odot}$ ) (see Figure 5, top-right panel). Among the data with no other spectral classification, we expect 23 AGNs instead of the 6 observed.

In order to reduce this discrepancy, 1-dimensional spectra are re-extracted from 2-dimensional frames, by integrating the counts on small apertures ( $\sim 5$  arcsec). These are labeled “mod-DS” (modified Drift-Scan) in Table 3 and are obtained in 22 cases out of the 190 available DS spectra. We re-extracted the spectra only for those galaxies with a significant enhancement in nuclear continuum emission or with clear inversion of the  $[\text{NII}]/\text{H}\alpha$  ratio in the two-dimensional spectrum, as in the case of VCC1401. The spectral classification of VCC524 changed from HII-like to Transition Objects; VCC596 passed from HII-like to Sey/LIN AGN; other 5 galaxies changed their classification from Transition Objects to Sey/LIN subclass. For all the others the classification remained unchanged. Owing to the existence of more suitable spectral material (the nuclear spectra, namely from

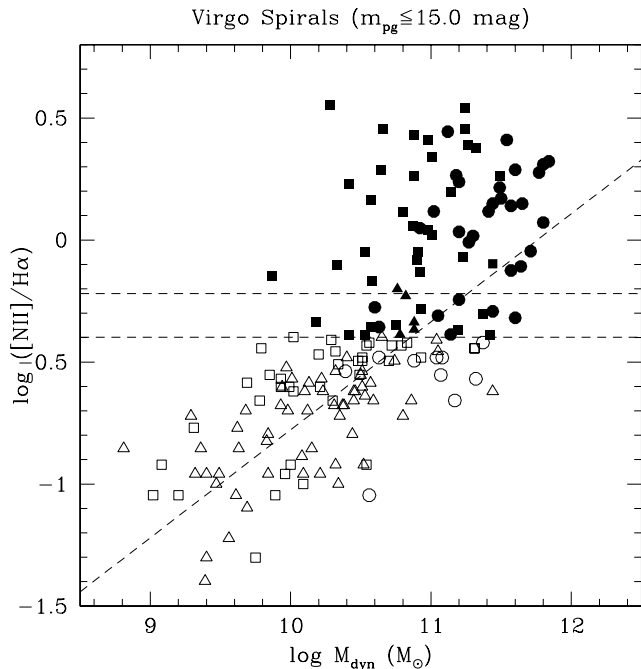


**Figure 6.** The dependence of  $[NII]/H\alpha$  on the dynamical mass separately for HII-like nuclei (empty symbols) and AGNs (filled symbols).

Ho, SDSS, Loiano) only 81 DS and 4 mod-DS spectra were adopted in the final classification.

By applying the same argument we expect to find 4 additional AGNs among the 24 galaxies that remain unclassified because the spectroscopic material is unavailable.

In conclusion we predict that once nuclear spectra will be available for the the whole sample, the number of AGNs in the Virgo cluster would increase at most by  $\sim 21$  units, over the presently known set of 77.

## 5 RESULTS

### 5.1 Nuclear activity versus dynamical mass

The data suggest that nuclear activity is very sensitive on the galaxy dynamical mass ( $M_{\text{dyn}}$ ). We observe that the frequency of AGNs increases very steeply with increasing  $M_{\text{dyn}}$ , a trend already apparent in Figure 2 (the symbol size, set proportional to  $M_{\text{dyn}}$ , increases toward the right-bottom angle of the Figure). Table 4 clearly shows that the majority of AGNs (89%) resides in galaxies more massive than  $10^{10.5} M_{\odot}$ .

Figure 6 shows the dependence of the  $[NII]/H\alpha$  ratio on the mass of the galaxies, that holds already for the HII like nuclei. This is a metallicity/luminosity relation well known since Lequeux et al. (1979); see also Zaritsky (1993) and Gavazzi et al. (2004). The linear regression for the HII like nuclei is drawn in Figure 6:

$$\log([NII]/H\alpha) = 0.44 \cdot \log M_{\text{dyn}} - 5.20 \quad (2)$$

It appears that nuclei classified as AGNs have a  $[NII]/H\alpha$  ratio significantly in excess of the relation found for HII nuclei. This provides a side-aspect, yet important when dealing with imaging surveys carried on with  $H\alpha$  filters (that

**Table 4.** AGN, HII and NEL statistics among 213 galaxies with available spectroscopic classification.

	AGN (77)	HII (121)	NEL (15)
$\log M < 10.5$	9 (12%)	84 (69%)	6 (40%)
$\log M \geq 10.5$	68 (88%)	37 (31%)	9 (60%)
Sa – Sb	41 (53%)	5 (4%)	11 (73%)
Sbc – Im – BCD	36 (47%)	116 (96%)	4 (27%)

are broad enough to contain the  $[NII]$  lines bracketing  $H\alpha$ ): there is a substantial, strongly mass dependent contribution from  $[NII]$  in the circumnuclear regions of galaxies. This reminds that significant (mass dependent) corrections to the  $H\alpha$  E.W. are needed to disentangle the contribution from  $[NII]$ ; otherwise, it would produce systematic overestimates of the  $H\alpha$  luminosity. This has relevant consequences for those studies that try to quantify the amount of circumnuclear star formation as a function of the local galaxy density using  $H\alpha$  imaging surveys (e.g. Moss & Whittle, 2005) or studies focused on  $H\alpha$  luminosity function (e.g. Pascual et al. 2001, Fujita et al. 2003, Ly et al. 2006;)

To further study and quantify the frequency of AGNs as a function of  $M_{\text{dyn}}$  let us consider the four histograms in Figure 7. The top-left histogram carries the frequency of AGNs, HII-like+NEL nuclei and the non classified (because their spectra are unavailable) objects. If we distribute the 24 non-measured ones according to the frequency of the measured galaxies, we obtain the top-right histogram showing a clear-cut dichotomy between HII-like and AGN nuclei at  $\log M_{\text{dyn}} \sim 10.5$ .

Once the AGNs are more finely divided into Transition, LINERs and Seyfert (bottom-left histogram; Sey/LIN objects are not plotted) there is a barely significant separation of these sub-components as a function of mass, because of the insufficient statistics (see the excellent analysis of SDSS data by Kewley et al. 2006). Finally the bottom-right histogram shows the differential fraction of AGNs emphasizing that below  $10^{10} M_{\odot}$  only one late type galaxy harbors an AGN, while above  $10^{11.5} M_{\odot}$  all do.

### 5.2 Nuclear activity versus galaxy morphology

As emphasized in Table 4, there is an obvious tendency for HII region-like nuclei to avoid early-type spirals and to inhabit late-type spirals (and vice versa for NEL galaxies). On the other hand, AGNs are almost as frequent in early and late-type spirals, i.e. the Hubble type does not appear to be the driver of the difference.

Figure 8 shows the Near-IR  $C_{31}$  (left) and the optical “nuclearity” (right) plotted as a function of  $M_{\text{dyn}}$  for galaxies in our sample, divided in normal (empty) and AGNs (filled). Albeit a general increase of the  $C_{31}$  with  $M_{\text{dyn}}$ , the two quantities are non-linearly correlated, as pointed out by Boselli et al. (1997), Gavazzi et al. (2000) and Scodreggio et al. (2002). There is in fact a number of very large mass ( $\log(M_{\text{dyn}}/M_{\odot}) > 11.5$ ) galaxies with very little bulges ( $C_{31} < 4$ ). AGNs inhabit high mass galaxies, not necessarily high  $C_{31}$  (Bulge-to-disk) ones. Clear-cut examples of bulge-less AGNs are M61, M100 and NGC4535, three Scs with  $\log(M_{\text{dyn}}/M_{\odot}) \sim 11.5$  and  $C_{31} \sim 2.5$ .

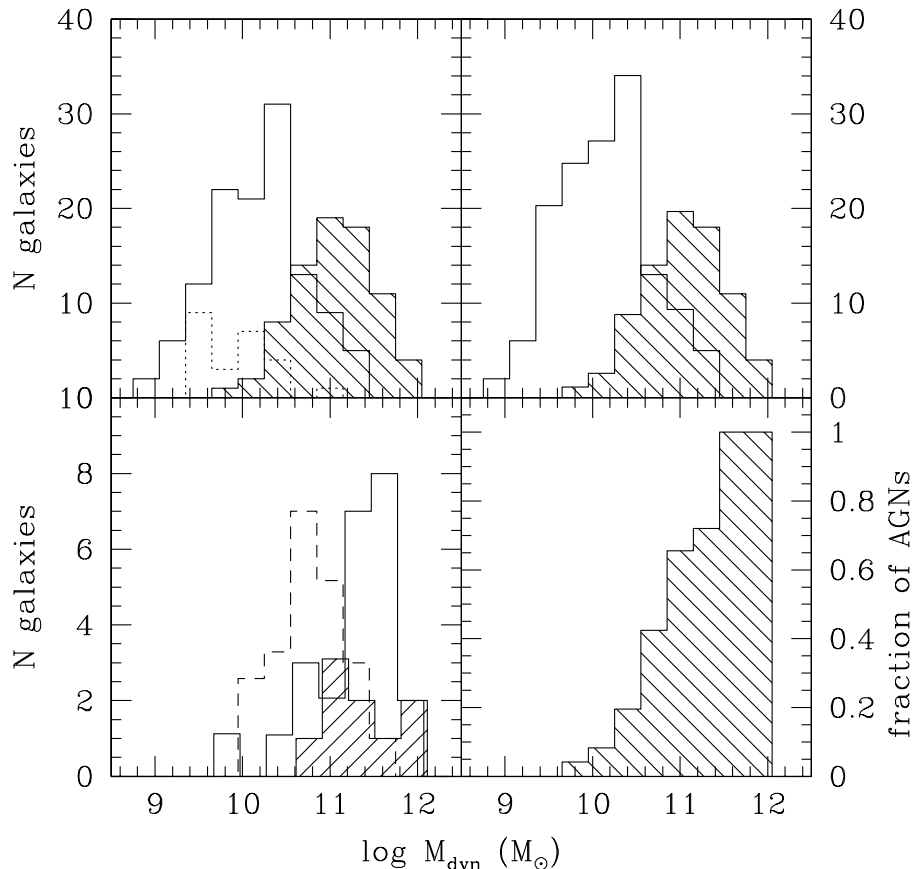


**Figure 7.** Histogram of the mass distribution of HII-like (continuous), AGNs (shaded) and not spectroscopically classified (top-left panel); same with the “not classified” distributed according to the frequency of the classified (top-right); blow-up of the AGNs divided in Seyfert (shaded), LINERs (continuous), and Transition (dashed) (bottom-left); fractional differential distribution of AGNs (bottom-right).

Conversely the right panel in Figure 8 shows that the presence of optical nuclei in the host galaxy increases with  $M_{\text{dyn}}$  as the fraction of AGNs. An optical nucleus may be due to the AGN continuum as well as to a steep enhancement in the concentration of stars. The first one would produce a power-law continuum. No DS nor SDSS spectrum showed such a behaviour. Spinelli et al. (2006) published high spatial resolution spectra obtained with HST (0.2 arcsec  $\approx$  16.4 pc in the Virgo Cloud A) of NGC4450, NGC 4698, M88 and M90, all having  $Nuc(r) > 1$ . Despite of the high resolution, no noticeable power law continuum is observed in the optical band. We thus conclude that the role of the AGN continuum is commonly negligible in our sample galaxies. Thus the galaxy dynamical mass seems to be the driver both for the formation of star nuclei, and for triggering the AGN. Notice that the massive, bulge-less Sc M61, M100 and NGC4535 have significant nuclei ( $Nuc(r) \sim 1.50$ ).

Obric et al. (2006) suggest that AGN host galaxies are mainly redder than star forming galaxies. This is interpreted as an evidence of feedback by the AGN on the host galaxy. AGNs do reside in red galaxies, as shown in Figure 9, but the existing and well-known color-magnitude correlation stands

for both active and non-active galaxies. The role of the AGN in halting star formation in the host galaxy is still debated.

### 5.3 Environmental dependencies

Kauffmann et al. (2004) find that in the SDSS the fraction of high luminosity AGNs (those with  $L[\text{OIII}] > 10^7 L_{\odot}$ ), predominant among type 2 Seyfert galaxies, depends on the environment, i.e. it decreases with increasing galaxy density, mimicking the behaviour of emission line galaxies. Conversely these authors find, in agreement with Miller et al. (2003), that the frequency of AGNs in general (dominated in number by low-luminosity LINERs) does not depend on the environment.

With a sample like the presently analyzed one, that is entirely made of galaxies members of a rich cluster, it is impossible to ensure that the estimate of the frequency of AGNs is not biased by the density of this particular environment. Neither we can perform a detailed study of environmental effects for each AGN subclass separately, due to the poor statistics.

Nevertheless we notice firstly that the overall fraction of AGNs associated with massive galaxies in the SDSS ( $> 80$

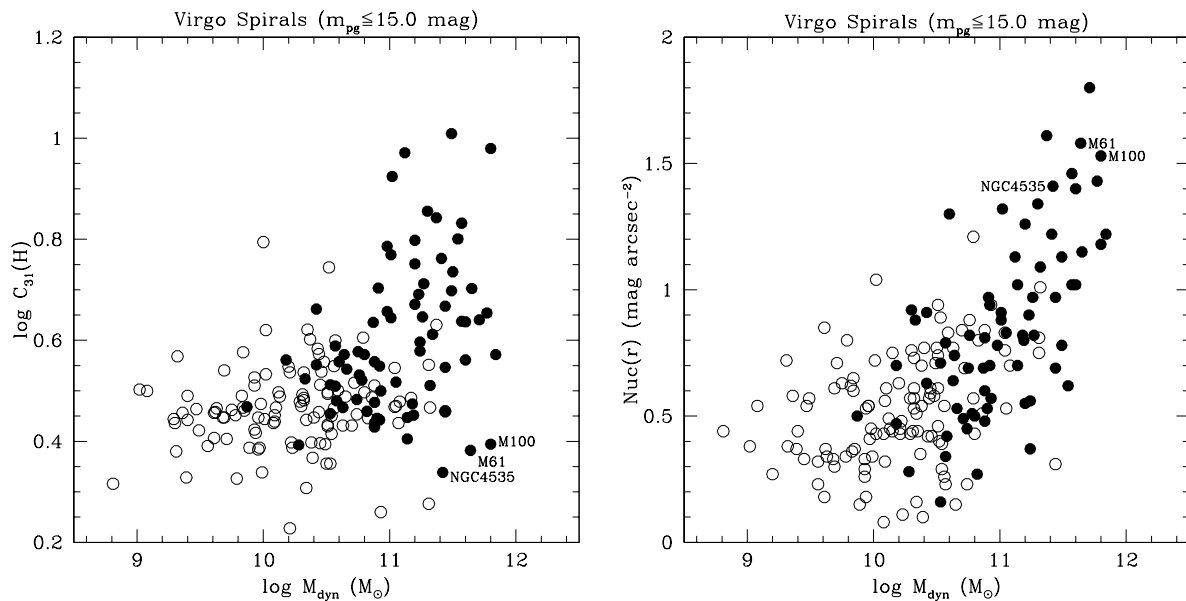


**Figure 8.** The Near-IR concentration index (left panel) and the  $r$ -band nuclearity index (right panel) as a function of the dynamical mass. Empty symbols are for HII region-like nuclei, filled symbols for all kinds of AGN, including transition objects. M61, M100 and NGC4535 are marked in both diagrams.

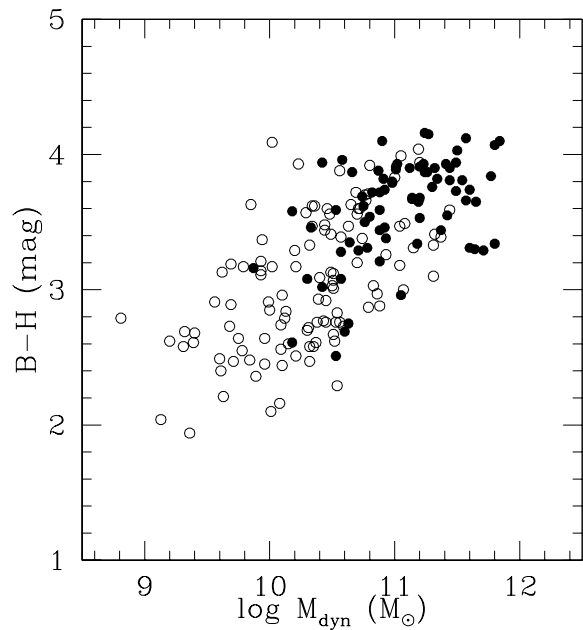


**Figure 9.** The dependence of B-H color on the dynamical mass of late-type galaxies with HII-like nuclei (empty symbols) and AGNs (filled symbols).

% for  $\log(M_{\text{stars}}/M_{\odot}) > 11$ , Kauffmann et al. 2003), is consistent with the one found in Virgo (see Figure 7)<sup>3</sup>. Such

<sup>3</sup> We transform  $M_{\text{stars}}$  used by the SDSS into  $M_{\text{dyn}}$  (within the optical radius) adopted in the present paper, using  $\log(M_{\text{stars}}/M_{\odot}) = 1.41 \times \log(M_{\text{dyn}}/M_{\odot}) - 5.1$ . This transformation is the linear correlation between  $\log M_{\text{dyn}}$  and  $\log M_{\text{stars}}$

a result is in contrast with Popesso & Biviano (2006). If we adopt an average galaxy velocity dispersion around 600 km/s for each Virgo Cloud (see Gavazzi et al. 1999), cut our sample at  $M_{\text{dyn}} \approx 6.3 \cdot 10^{10} M_{\odot}$  (roughly corresponding to  $M_{\text{pg}} \approx -20$ ), and adopt the same limits in classifying the nuclear activity, our AGN fraction reaches 60%, nearly a  $2 \sigma$  deviation from their correlation. We argue that the reason of such a difference resides in the sample selection. Unlike Kauffmann et al. (2003), the sample of Popesso & Biviano has no constraints on line fluxes. Thus, it includes lots of No Emission Line galaxies, especially among early-type, gas poor galaxies for which the BPT classification may be unavailable.

Secondly we remark that, if we divide the Virgo sample in two subsamples composed of galaxies in and outside 5 degrees ( $\sim 1.5$  Mpc) projected radial distance from M87, we obtain that the percentage of AGNs varies from  $32 \pm 8\%$  “in” to  $40 \pm 10\%$  “out”, i.e. not significantly. The lack of an environmental dependence of our sample AGNs is illustrated in Figure 10. Similarly by dividing the sample using an independent probe of the environmental influence, as represented by the Hydrogen deficiency parameter (see the parameter definition in Haynes & Giovanelli, 1984 and Boselli & Gavazzi, 2006), we obtain that the percentage of AGNs varies from  $41 \pm 13\%$  among highly deficient objects ( $Def_{\text{HI}} > 0.5$ ), to  $27 \pm 7\%$  among the unperturbed objects ( $Def_{\text{HI}} \leq 0.5$ ), i.e. barely significantly (see figure 11). We thus conclude that the frequency of AGNs is not strongly environment dependent.

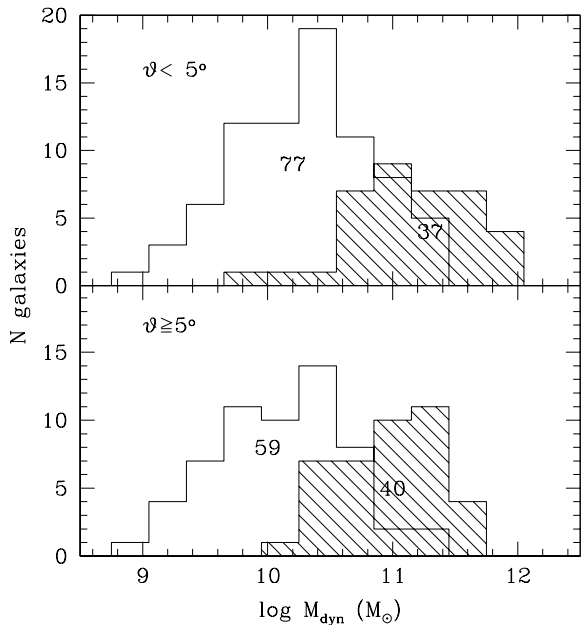


**Figure 10.** The observed distribution of AGNs (shaded) and HII region-like+NEL nuclei (thick histogram) as a function of  $M_{\text{dyn}}$ , given separately for galaxies found within (top) or outside (bottom) 5 degrees projected radial distance from M87.

#### 5.4 Indirect estimate of black hole masses and Eddington ratios

With the current data it is not possible to directly infer the mass of the black holes that power the AGNs observed in our sample. We may nevertheless consider the possibility of extending the known scale relations valid for spheroids to the bulges and optical nuclei of our late-type galaxies. The relations used in this section are the  $M_{\text{BH}} - \sigma$  (Tremaine et al., 2002 and references therein) and the  $M_{\text{BH}} - L_{\text{bulge}}(\text{H})$  (Marconi & Hunt, 2003). Data on the stellar velocity dispersion  $\sigma$  are taken from hypercat<sup>4</sup> when available for the AGN sample. The values for  $\sigma$  are estimated using various techniques (mainly the Fourier quotient method). Data on the bulge luminosity are taken from Gavazzi et al. (2000). The bulge luminosity is estimated from the deconvolution of the galaxy light profile in H-band. The light profile is modeled as a de Vaucouleurs or an exponential curve for the bulge and an exponential law for the disk component. Since the AGN continuum flux is found to be negligible in our sample galaxies, and the fit procedure is performed only out of the first two seeing radii, we disregarded the AGN contribution in the fit. Typical values for the Bulge to Total luminosity ratio (B/T) varies between few % to 30%. A reasonable estimate of the bulge luminosity error is around 30%. Twenty and 64 out of 77 AGNs in our sample have data for these two estimates to be performed; this subsample includes, for example, M100 with its optical nucleus and M58 which hosts a prominent bulge. Figure 12 shows the comparison between the black hole mass estimates obtained with the two methods. The slight (0.4 dex) offset between the two estimates

<sup>4</sup> <http://leda.univ-lyon1.fr>

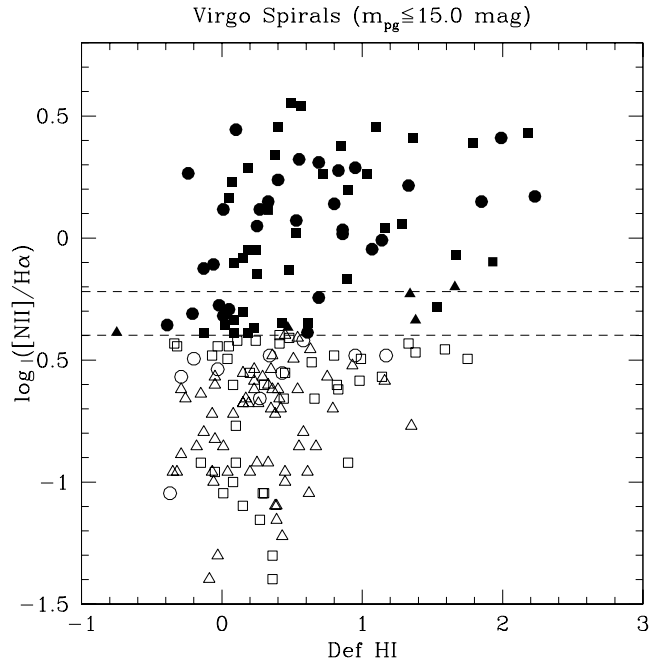


**Figure 11.** [NII]/H $\alpha$  ratio plotted versus Hydrogen deficiency, as defined in Haynes & Giovanelli (1984). The AGN fraction increases only slightly from non-deficient to deficient galaxies.

may depend on the heterogeneous data sources adopted for  $\sigma$  estimates, or on the bulge luminosity underestimate due to inclination. Since we want to study the black-hole masses and the Eddington ratios of Virgo AGNs only from a statistical point of view, and the data dispersion is higher, such an offset is irrelevant for the purposes of our analysis. We notice that the two methods provide consistent values of the black hole mass for M100 as well as for M58. This result is surprising given the difference between M100 and M58, the first hosting a pseudobulge/optical nucleus (Kormendy & Kennicutt, 2004; see also Allard et al., 2006) while the second a massive extended bulge: this coincidence highlights the close underlying connection between the stellar velocity dispersion and the nuclear or bulge luminosity in these two galaxies.

As shown in Figure 12 the black hole masses never exceed a few  $10^8$  solar masses, and a number of galaxies hosts relatively light black holes ( $M_{\text{BH}} \lesssim 10^7 M_{\odot}$ ). These black holes appear to fill the low mass end of the scaling relation purely sampled in our Local Universe.

Black hole masses may provide some hints on the Eddington ratios of the AGNs if we have a way to estimate the bolometric luminosity of the active BH. Since most of our AGN are LINERs, it is difficult to disentangle the emission of the AGN from that of the stellar continuum in the optical band. As proposed in Heckman et al. (2004) (see also Kauffmann & Heckman, 2005), we can estimate the AGN bolometric luminosity from the [OIII] emission line flux. We want to stress that this is a rough estimate of bolometric luminosities, since a good spectrometric calibration is often hard to achieve, because of the diffuse nature of the source, and contamination from other ionizing radiation sources is often present. Combining the data on the [OIII] flux from Ho and SDSS, and matching them with the subsample of the

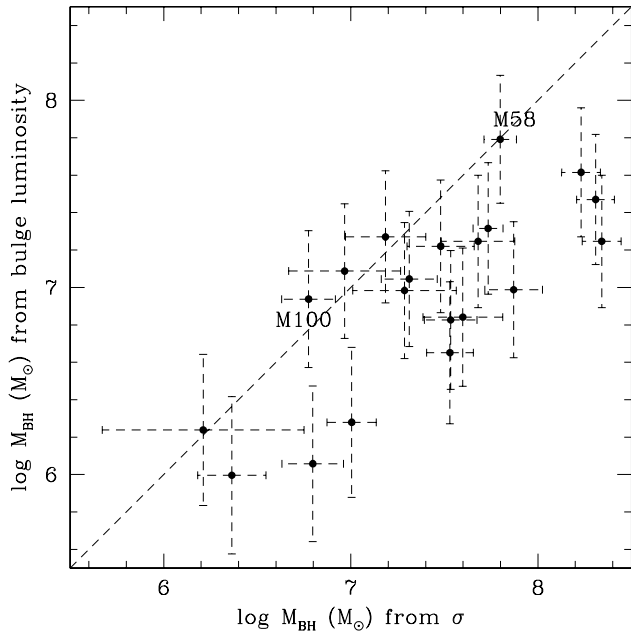


**Figure 12.** Comparison between  $M_{\text{BH}}$  estimated using the  $M_{\text{BH}} - \sigma$  relation (Tremaine et al., 2002) ( $x$  axis) and  $M_{\text{BH}}$  from the  $M_{\text{BH}} - L_{\text{bulge}}$  (Marconi & Hunt, 2003) ( $y$  axis). Uncertainties in the relations are accounted for in our error bars; for  $L_{\text{bulge}}$  we assumed a 30 % error both on the Bulge to Total value and on total NIR Luminosity.

AGN BH masses, we infer the bolometric to Eddington luminosity ratios of 33 of our AGNs (we could not use Loiano spectra since they do not include [OIII] line, neither drift scan spectra since they lack of an absolute spectrophotometric calibration). The mean error of Heckman’s bolometric correction is 0.38 dex, thus our Eddington ratios mean error is nearly 0.5 dex. These ratios are found to fall in the range  $10^{-5} - 10^{-2}$  with a mean around 0.001, indicating that these AGN are accreting at very low rates (see Figure 13). The only exceptions are NGC4388, with Eddington ratio of 0.06 which reflects the occurrence of ejection in this source (see Yoshida et al., 2004), and NGC4123, a LIN/HII object, in which O,B-stars ionization is probably significant.

## 6 CONCLUSIONS

The present study focused on the nuclear activity of spiral galaxies in the Virgo cluster, as representative of our Local Universe. This paper provides the first census of AGNs associated to the cluster’s spirals, complete down to the 15<sup>th</sup> magnitude. This allowed the identification of a number of low luminosity AGNs even in late type spirals that show a bright optical stellar nucleus rather than a prominent bulge: M100 hosts a LINER and offers a clear example.

A first result is that the AGNs, and among them LINERs, are primarily associated to the spirals with dynamical mass in excess of  $M \gtrsim 10^{10} M_{\odot}$ . This result is in close agreement with Kauffmann et al. (2003) who found that AGNs in the SDSS are hosted in galaxies (with mean redshift  $\sim 0.1$ ) as massive as ours.

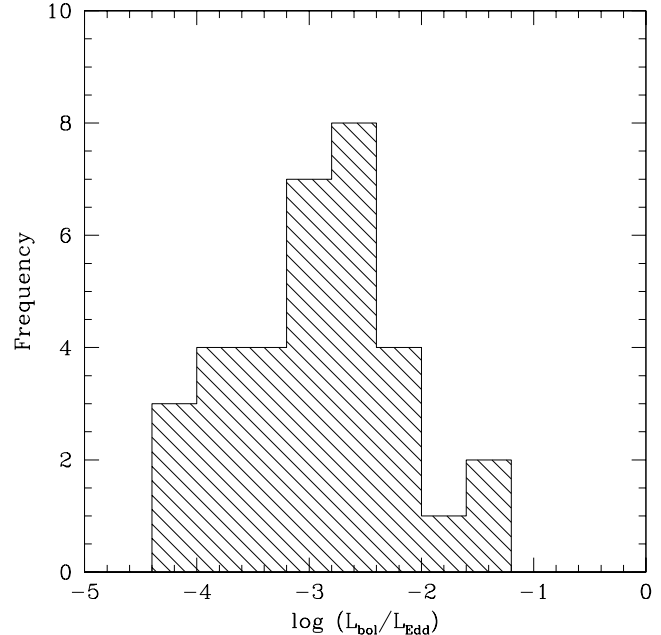


**Figure 13.** Eddington ratio distribution in a subset of AGNs in our sample. The Marconi & Hunt relation was applied to estimate black hole masses and Eddington luminosities.

In particular, we found the fraction of AGNs in late-type galaxies more massive than  $\sim 10^{8.5} M_{\odot}$  is  $77/237 \approx 32\%$ . This fraction steeply increases with the galaxy mass: if we consider only galaxies with  $M_{\text{dyn}} > 10^{11.5} M_{\odot}$ , the AGN fraction approaches 100 %.

A second result is that the presence of nuclear activity is insensitive to the morphological type of the host spiral, as it is equally present in Sa - Sb and later types. Thus, M100 is not an isolated case. AGNs are often associated to prominent stellar nuclei. In addition, the nuclear activity displays little or no environmental density dependence inside the cluster, neither as a function of the host galaxy position within the cluster, nor of the neutral gas deficiency. Gas accretion onto central BHs seems independent of the gaseous content.

As already pointed out, the nuclear activity occurs in spiral galaxies with dynamical masses above  $\sim 10^{10} M_{\odot}$ , and the fraction of  $M_{\text{dyn}}$  in the spheroidal component in spirals varies between a few % to 30 %. If we apply the known black hole scaling relations, obeyed in ellipticals, to the bulges and optical nuclei of our sample (thus assuming self-similarity among early and late type galaxies), this translates into a lower limit for the black hole mass of  $\sim 10^6 M_{\odot}$ . Based on AGN luminosity function evolution, Marconi et al. (2006) have suggested that also the black holes grow following the galaxy downsizing, i.e. massive black holes grow faster and earlier with cosmic time than the lighter ones. If black holes lighter than  $10^6 M_{\odot}$  are hosted in spirals with less prominent nuclei/bulges, we would have expected them still in their active phase in the galaxies inside our census. The lack of AGNs in lower mass spirals may be a hint that such lighter BHs did not find yet the right conditions to grow or the environment to form. This dichotomy on the BH behaviour around  $10^6 M_{\odot}$  has to be considered valid at a statistical level.

It is interesting to notice that ACS imaging surveys on elliptical galaxies have shown that a sizeable fraction of low and intermediate luminosity ellipticals contain stellar cusps at their center with masses in the range expected from the lower-end extrapolation of the  $M_{\text{BH}} - \text{Magnitude}$  correlation (Wehner & Harris, 2006; Ferrarese et al. 2006b). Above  $10^{10} M_{\odot}$  ellipticals host exclusively massive black holes. Similarly, in our sample of spirals, we have not found at statistical level an active AGN below such a characteristic dynamical mass once we correct for the total to bulge ratio. This is a hint that below a critical mass for the hosting spheroidal component (either a bulge or a stellar nucleus), lighter black holes become rarer.

Only a relatively small sample of black holes in spiral galaxies have a direct mass measure. In this paper we found the occurrence of BHs at the center of spiral galaxies disregarding of the galaxy morphology, and we provided an estimate of the black hole mass under the assumption of self-similarity between the bulges and stellar nuclei of our spirals with the sample of quiescent black hole hosted in ellipticals. We do not know if this similarity applies, since either in the black hole mass as well as in the mass accretion rate there might be a dependence on the angular momentum of the host spiral that can affect black hole grow. Further high resolution observations focused on black hole mass measures in late-type galaxies may provide clues on the applicability of the  $M_{\text{BH}} - \text{bulge}$  relations and the role of the both the Bulge to Total ratio and the dynamic of the gas and stars in the host galaxy.

### Acknowledgements

We thank F. Haardt and A. Treves for useful discussions. G.G. thanks A. A. for inspiring hints. This research has made extensive use of the GOLDMine Database (Gavazzi et al. 2003). We acknowledge the usage of the HyperLeda database (Paturel et al. 2003). This research has made use of the NASA/IPAC Extragalactic Database (NED) which is operated by the Jet Propulsion Laboratory, California Institute of Technology, under contract with the National Aeronautics and Space Administration.

### REFERENCES

- Adelman-McCarthy, J., et al. 2007, submitted to ApJ Supplements
- Allard, E. L., Knapen, J. H., Peletier, R. F., Sarzi, M., 2006, MNRAS, 371, 1087
- Baldwin, J. A., Phillips, M. M., Terlevich, R., 1981, PASP, 93, 5
- Bennert, N., et al., 2006, A&A, 446, 919
- Binggeli, B., Sandage, A., & Tammann, G., 1985, AJ, 90, 1681
- Binggeli, B., Popescu, C. & Tammann, G., 1993, AAS, 98, 275
- Boselli, A., Tuffs, R. J., Gavazzi, G., Hippelein, H., Pierini, D., 1997, A&AS, 121, 507
- Boselli, A., Boissier, S., Cortese, L., Gil de Paz, A., Seibert, M., Madore, B. F., Buat, V., Martin, D. C., 2006, ApJ, 651, 811
- Boselli, A. & Gavazzi, G., 2006, PASP, 118, 517
- Bruzual, G. & Charlot, S. 2003, MNRAS, 344, 1000
- Chyży, K. T., Soida, M., Bomans, D. J., Vollmer, B., Balkowski, Ch., Beck, R., Urbanik, M., 2006, A&A, 447, 465
- Cote', P., et al, 2006, ApJS, 165, 57
- Dressler, A., Thompson, I. B., Sheckman, S. A., 1985, ApJ, 288, 481
- Ferrarese, L., et al., 2006a, ApJS, 164, 334
- Ferrarese, L., et al., 2006b, ApJ, 644L, 21
- Filho, M. E., Fraternali, F., Markoff, S., et al., 2004, A&A, 418, 429
- Fujita, S.S., Ajiki, M., Shioya, Y., et al., 2003, ApJ, 586L, 115
- Garca-Burillo, S., Combes, F., Schinnerer, E., Boone, F., Hunt, L. K., 2005, A&A, 441, 1011
- Gavazzi, G., Pierini, D., & Boselli, A., 1996, A&A, 312, 397
- Gavazzi, G., Boselli, A., Scodreggio, M., et al., 1999, MNRAS, 304, 595
- Gavazzi, G., Franzetti, P., Scodreggio, M., et al., 2000, A&A, 361, 863
- Gavazzi, G., Zibetti, S., Boselli, et al., 2001, A&A, 372, 29
- Gavazzi, G., Boselli, A., Donati, A., et al., 2003, A&A, 400, 451
- Gavazzi, G., Zaccardo, A., Sanvito, G., et al., 2004, A&A, 417, 499
- Gavazzi, G., et al., 2006, A&A, 446, 839
- Halderson, E. L., Moran, E. C., Filippenko, A. V., Ho, L. C., 2001, AJ, 122, 637
- Hao, L., Strauss, M.A., Tremonti, C.A., et al. 2005, ApJ, 129, 1783
- Haynes, M. & Giovanelli, R., 1984, AJ, 89, 758
- Heckman, T.M., Kauffmann, G., Brinchmann, J., et al., 2004, ApJ, 613, 109
- Ho, L.C., Filippenko, A.V., & Sargent, W.L.W., 1997, ApJS, 112, 315
- Kauffmann, G., et al. 2003, MNRAS, 346, 1055
- Kauffmann, G., White, S.D.M., Heckman, T. M., et al. 2004, MNRAS, 353, 713
- Kauffmann, G., Heckman, T.M., 2005, RSPTA, 363, 621
- Kewley, L.J., Dopita, M.A., & Southerland, R.S., et al. 2001, ApJ, 556, 121
- Kewley, L.J., Groves, B., Kauffmann, G., Heckman, T., 2006, MNRAS, 372, 961
- Kormendy, J., & Kennicutt, R.C., 2004, ARA&A, 42, 603
- Lequeux, J., Peimbert, M., Rayo, J. F., Serrano, A., Torres-Peimbert, S., 1979, A&A, 80, 155
- Ly, C., Malkan, M., Kashikawa, N., et al., 2006, AAS, 208, 5302
- Marconi, A. & Hunt, L., 2003, ApJ, 589, 21
- Marconi, A., Comastri, A., Gilli, R., Hasinger, G., Hunt, L.K., Maiolino, R., Risaliti, G., Salvati, M., 2006, MmSAI, 77, 742
- Martini, P., Kelson, D., Kim, E., et al., 2006, ApJ, 644, 116
- Miller, C.J., Nichol, R.C., Gómez, P.L., Hopkins, A.M., Bernardi, M., 2003 ApJ, 597, 142
- Moss, C. & Whittle, M., 2005, MNRAS, 357, 1337
- Pascual, S., Gallego, J., Aragón-Salamanca, A., Zamorano, J., 2001, A&A, 379, 798
- Paturel, G., et al., 2003, A&A, 412, 45
- Popesso, P., & Biviano, A., 2006, A&A, 460, L23
- Shen, Y., Mulchaey, J.S., Raychaudhury, S., et al., 2007, ApJ, 654, L115

- Spinelli, P.F., Storchi-Bergmann T., Brandt C.H., Calzetti, D., 2006, *ApJ*, 166, 498
- Stasińska, G., Cid Fernandes, R., et al., 2006, *MNRAS*, 371, 972
- Scodeggio, M., Gavazzi, G., Franzetti, P., et al., 2002, *A&A*, 384, 812
- Terashima, Y., Iyomoto, N., Ho, L., Ptak, A., 2002, *ApJS*, 139, 1
- Tremaine, S., Gebhardt, K., Bender, R., et al., 2002, *ApJ*, 574, 740
- Veilleux, S., & Osterbrock, D.E., 1987, *ApJS*, 63, 295
- Veilleux, S.; Shopbell, P. L.; Rupke, D. S.; Bland-Hawthorn, J.& Cecil, G, 2003, *AJ*, 126, 2185
- Wehner, E.H., Harris, W.E., 2006, *ApJ*, 644L, 17
- York, D.G.; Adelman, J.; Anderson, J.E.; et al. 2000, *AJ*, 120, 1579
- Yoshida, M., Ohyama, Y., Iye, M., et al., 2004, *AJ*, 127, 90
- Zaritsky, D., 1993, *PASP*, 105, 1006

Table 5: spectroscopic results

VCC/CGCG	NGC	TYPE	$m_{pg}$ mag (4)	$D$ Mpc (5)	$\log L_H$ $L_\odot$ (6)	$C_{31}(H)$ (7)	$Nuc(r)$ mag arcsec $^{-2}$ (8)	[NII]/H $\alpha$ (9)	[OIII]/H $\beta$ (10)	Spec Class (11)	Ref (12)
1	-	BCD	14.78	32	9.27	3.36	0.29	0.27	0.48	HII	SDSS
10	-	BCD	14.75	32	9.27	2.65	0.33	0.25	0.71	HII	SDSS
15	-	Sa	14.70	32	-	-	-	0.45	-	LIN/HII	SDSS
24	-	BCD	14.95	32	9.34	6.23	-	0.12	2.37	HII	SDSS
25	4152	Sc	12.46	32	10.39	3.29	0.83	0.32*	0.51*	LIN/HII	Ho
47	4165	Sa	14.20	32	10.09	3.78	0.69	0.45	-	LIN/HII	SDSS
58	-	Sb	13.17	32	10.17	2.79	0.8	0.38	-	HII	SDSS
66	4178	Sc	11.89	17	10.22	3.24	0.84	0.19*	1.37*	HII	Ho
67	-	Sc	13.98	32	9.86	5.55	0.4	0.12*	-	HII	DS
73	4180	Sb	13.35	32	10.58	3.79	0.56	2.84	-	Sey/LIN	LOI
87	-	Sm	15.00	17	8.36	3.18	0.38	0.09	2.09	HII	SDSS
89	4189	Sc	12.53	32	10.65	1.89	0.81	0.36	0.14	HII	SDSS
92	4192	Sb	10.92	17	10.99	5.04	1.15	1.29	-	LIN	Ho
97	4193	Sc	13.20	32	10.53	2.83	0.8	0.43	0.42	LIN/HII	SDSS
105	-	Sd	13.68	32	-	-	0.64	0.27*	-	HII	DS
119	-	Sd	14.76	32	-	-	0.19	0.08	1.28	HII	SDSS
120	4197	Scd	13.47	32	10.20	3.07	0.51	0.22*	1.14*	HII	DS
126	-	Sd	14.42	17	-	-	-	-	-	NEL	SDSS
131	-	Sc	14.34	17	9.52	3.64	0.47	0.46	-	LIN/HII	SDSS
135	-	S/BCD	14.81	32	9.82	3.61	0.58	0.32	-	HII	SDSS
145	4206	Sc	12.77	17	9.98	3.73	0.74	1.93	-	LIN	SDSS
152	4207	Scd	13.48	17	9.90	3.54	0.54	0.38	0.45	HII	SDSS
157	4212	Sc	11.50	17	10.48	2.54	0.7	0.35*	-	LIN/HII	Ho
162	-	Sd	14.41	17	9.23	2.44	0.15	0.09	1.83	HII	SDSS
167	4216	Sb	10.97	17	11.14	9.54	1.18	3.27	-	LIN	Ho
170	-	Sd	14.56	17	9.03	2.80	0.61	0.26	0.49	HII	SDSS
172	-	BCD	14.50	32	9.30	2.80	0.54	0.11	4.28	HII	SDSS
187	4222	Scd	13.91	17	9.57	2.44	0.11	0.24*	0.88*	HII	DS
199	4224	Sa	12.95	32	10.83	4.99	0.78	-	-	Sey/LIN	LOI
213	-	S/BCD	14.26	17	9.21	2.94	0.5	0.71	-	LIN	SDSS
221	4234	Sc	13.43	32	9.88	2.60	0.39	0.37	0.48	HII	SDSS
222	4235	Sa	12.62	32	10.88	6.32	0.62	-	-	Sey	Ho
224	-	Scd	14.70	17	9.19	2.89	0.37	0.28	0.62	HII	SDSS
226	4237	Sc	12.53	17	10.26	2.77	0.7	0.74	-	Sey/LIN	SDSS
227	-	Sdm	14.90	32	9.44	3.17	-	-	-	NEL	SDSS
234	4241	Sa	12.99	32	10.68	4.09	-	7.69	-	Sey/LIN	MDS
241	-	Sd	14.60	17	-	-	0.35	0.04	3.37	HII	SDSS
267	-	Sbc	13.82	23	9.72	2.50	0.54	0.21*	-	HII	DS
289	4252	Sc	14.81	32	9.33	2.18	0.34	0.25	3.85	HII	SDSS
307	4254	Sc	10.43	17	10.94	3.64	1.02	0.33*	0.22*	LIN/HII	Ho
315	-	Sa	14.98	32	9.70	-	-	-	-	NEL	SDSS
318	-	Scd	14.01	32	9.18	2.93	0.6	0.16*	1.68*	HII	DS
323	4257	Sa	14.91	32	10.00	3.49	0.53	2.84	-	LIN	SDSS
324	-	BCD	14.78	17	9.09	2.90	0.63	0.05	3.88	HII	SDSS
340	-	BCD	14.43	32	9.43	2.83	0.32	0.10	2.37	HII	SDSS
341	4260	Sa	12.70	23	10.60	4.43	0.97	2.46	-	Sey/LIN	SDSS
358	4264	Sa	13.80	23	10.03	3.76	-	-	-	NEL	SDSS
382	4273	Sc	12.37	32	10.65	3.56	0.75	0.36	-	HII	LOI
386	4277	Sa	14.47	32	10.05	3.46	-	-	-	NEL	DS
393	4276	Sc	13.25	23	9.85	2.69	0.74	0.25*	-	HII	DS
404	-	Scd	15.00	17	9.36	3.41	0.43	0.40	-	HII	SDSS
415	-	Sd	14.82	23	-	-	0.28	-	-	HII	DS
459	-	BCD	14.95	17	8.74	3.09	0.44	0.11*	2.88*	HII	DS
460	4293	Sa	11.20	17	10.78	3.52	0.97	4.19	-	LIN	Ho
465	4294	Sc	12.62	17	9.88	2.82	0.29	0.12	1.94	HII	SDSS
483	4298	Sc	12.08	17	10.42	3.01	0.7	0.35	0.23	HII	Ho
491	4299	Scd	12.86	17	9.42	2.73	0.08	0.13*	2.05*	HII	DS
492	4300	Sa	13.76	23	10.21	4.32	0.69	1.14	-	Sey/LIN	LOI
497	4302	Sc	12.55	17	10.58	3.95	0.37	3.49	-	Sey/LIN	SDSS
508	4303	Sc	10.17	17	10.98	2.41	1.58	0.41*	0.28*	LIN	Ho
509	-	Sdm	14.98	23	-	-	0.54	-	-	HII	DS
522	4305	Sa	13.19	17	9.83	3.00	-	-	-	NEL	SDSS
524	4307	Sbc	12.79	23	10.27	3.16	0.57	0.52	0.28	LIN/HII	MDS
534	4309	Sa	13.59	23	10.10	3.63	0.88	-	-	NEL	DS
552	-	Sc	13.61	17	9.05	2.54	0.71	-	-	HII	DS
559	4312	Sab	12.56	17	10.22	3.61	0.48	0.46*	-	LIN/HII	DS
568	-	S..	14.91	23	-	-	0.28	0.11*	-	HII	DS
570	4313	Sab	12.73	17	10.32	4.54	-	2.26	-	Sey/LIN	SDSS
576	4316	Sbc	13.70	23	10.24	2.79	0.53	0.83	-	Sey/LIN	SDSS
596	4321	Sc	10.11	17	11.14	2.48	1.53	0.66	-	LIN	Ho
613	4324	Sa	12.60	17	10.35	4.41	0.91	2.34	-	Sey/LIN	LOI
630	4330	Sd	13.10	17	9.91	3.98	0.23	0.26*	-	HII	DS
655	4344	S/BCD	13.21	17	9.56	2.50	0.48	0.27*	0.17*	HII	DS
656	4343	Sb	13.14	23	10.35	5.88	0.88	1.05	-	Sey/LIN	LOI
664	-	Sc	13.50	17	8.95	2.55	0.85	0.09*	2.68*	HII	DS
667	-	Sc	14.24	23	9.78	3.74	0.57	0.16*	-	HII	DS
675	-	Sa	15.00	17	8.54	-	0.27	0.09	2.77	HII	SDSS
688	4353	Sc	13.94	23	9.68	2.03	0.16	0.10*	-	HII	DS
692	4351	Sc	12.93	17	9.64	2.95	0.76	0.22	0.28	HII	SDSS
699	-	Pec	14.22	23	9.71	4.00	0.35	0.21*	1.31*	HII	DS
713	4356	Sc	14.04	23	10.16	2.88	0.27	0.59*	-	LIN/HII	DS
737	-	S/BCD	14.94	17	8.73	2.13	0.37	-	-	HII	DS
739	-	Sd	14.37	17	8.65	2.40	0.72	0.17	1.11	HII	SDSS
785	4378	Sa	12.16	17	10.46	9.36	1.13	-	-	Sey	Ho
787	4376	Scd	13.69	23	9.65	3.11	0.44	0.21*	-	HII	DS
792	4380	Sab	12.36	23	10.66	3.24	1.09	2.38	-	Sey/LIN	SDSS
809	-	Sc	14.55	17	9.27	3.24	0.26	0.21*	0.85*	HII	DS
827	-	Sc	13.76	23	10.14	3.14	0.43	0.19*	1.80*	HII	DS
836	4388	Sab	11.83	17	10.54	4.69	0.55	0.56	11.34	Sey	Ho
848	-	16	14.72	23	8.70	2.86	0.58	0.14*	2.05*	HII	DS
849	4390	Sbc	13.27	23	9.79	2.49	0.59	0.22*	0.94*	HII	DS
851	-	Sc	14.14	23	9.80	3.45	0.42	0.24*	0.77*	HII	DS
857	4394	Sb	11.76	17	10.54	5.64	1.26	1.02	-	LIN	Ho
859	-	Sc	14.61	17	9.62	2.47	0.28	3.58	-	Sey/LIN	SDSS
865	4396	Sc	13.02	17	9.69	4.18	0.44	0.19*	0.97*	HII	DS
873	4402	Sc	12.56	17	10.39	2.95	0.53	0.35*	-	HII	DS
874	4405	Sc	12.99	17	9.97	2.70	0.77	0.37	-	HII	Ho
905	-	Sc	13.42	23	9.66	3.06	0.53	0.29*	0.71*	HII	DS
912	4413	Sbc	12.97	17	9.85	3.14	0.94	0.32	-	HII	LOI
921	4412	Sbc	13.14	17	9.64	2.19	0.92	0.42*	0.31*	LIN	NED
938	4416	Sc	13.28	17	9.74	2.80	0.77	0.33*	0.20*	HII	DS
939	-	Sc	12.92	23	9.87	3.25	0.71	0.89	-	Sey/LIN	SDSS
950	-	Sm	14.49	17	8.63	2.78	-	0.19*	-	HII	DS
957	4420	Sc	12.67	17	9.91	3.23	0.34	0.44	0.62	LIN/HII	SDSS
958	4419	Sa	12.13	17	10.61	5.15	0.82	1.61	-	LIN	Ho
971	4423	Sd	14.28	23	9.55	3.44	0.43	0.11*	1.91*	HII	DS

Table 5: spectroscopic results

VCC/CGCG	NGC	TYPE	$m_{pg}$ mag	$D$ Mpc	$\log L_H$ $L_\odot$	$C_{31}(H)$	$Nuc(r)$ mag arcsec $^{-2}$	[NII]/H $\alpha$	[OIII]/H $\beta$	Spec Class	Ref
(1)	(2)	(3)	(4)	(5)	(6)	(7)	(8)	(9)	(10)	(11)	(12)
975	-	Scd	13.58	23	9.66	3.03	0.61	0.12*	-	HII	DS
979	4424	Sa	12.32	23	10.38	3.51	0.83	0.34	0.20	HII	Ho
980	-	Scd	14.17	17	8.15	2.07	0.44	0.14*	1.71*	HII	DS
984	4425	Sa	12.82	17	10.11	4.68	-	-	-	NEL	SDSS
1002	4430	Sc	12.48	23	10.22	2.73	0.81	0.43*	-	LIN/HII	DS
1011	-	Sdm	14.85	17	8.90	2.46	0.23	-	-	HII	DS
1043	4438	Sb	10.91	17	10.83	10.21	1.13	1.97	-	LIN	Ho
1047	4440	Sa	12.48	17	10.34	7.42	-	-	-	NEL	DS
1060	-	Sm	15.00	17	-	-	0.37	0.07	1.60	HII	SDSS
1086	4445	S..	13.66	23	10.08	3.04	0.45	-	-	LIN/HII	DS
1091	-	Sbc	14.60	23	9.18	3.77	0.65	0.11*	2.28*	HII	DS
1110	4450	Sab	10.93	17	10.94	4.33	1.4	6.74	-	LIN	Ho
1118	4451	Sc	13.31	23	10.08	2.84	0.23	0.32*	0.17*	HII	DS
1126	-	Sc	13.30	17	10.06	3.28	0.69	0.37	-	HII	SDSS
1145	4457	Sb	11.66	17	10.64	7.17	1.34	3.25	-	LIN	Ho
1156	-	Scd	14.13	17	-	-	0.43	-	-	HII	SDSS
1158	4461	Sa	12.09	17	10.54	7.45	-	-	-	NEL	DS
1189	-	Sc	13.70	17	9.30	2.42	0.54	-	-	HII	DS
1190	4469	Sa	12.22	23	10.78	4.65	0.69	0.8	-	Sey/LIN	SDSS
1193	4466	Sc	14.62	17	9.28	2.61	0.18	0.25*	0.71*	HII	DS
1205	4470	Sc	13.04	17	9.73	2.33	0.1	0.26*	0.51*	HII	Ho
1217	-	Sm	14.59	17	8.94	2.80	-	-	-	NEL	DS
1249	-	Im	14.75	17	8.47	2.73	-	-	-	NEL	DS
1266	-	Sdm	14.63	17	-	-	-	-	-	HII	SDSS
1290	4480	Sb	13.09	17	9.91	3.88	0.79	1.46	-	Sey/LIN	SDSS
1326	4491	Sa	13.41	17	9.78	2.87	-	-	-	HII	DS
1330	4492	Sa	13.17	17	10.13	4.41	1.21	-	-	NEL	LOI
1375	-	Sc	12.00	17	9.35	2.78	0.72	0.27*	0.54*	HII	DS
1379	4498	Sc	12.62	17	9.84	2.27	0.77	0.28*	0.28*	HII	DS
1393	-	Sc	14.01	17	9.47	3.08	0.45	0.26*	0.31*	HII	DS
1401	4501	Sbc	10.27	17	11.18	3.73	1.22	1.42	-	Sey	Ho
1410	4502	Sm	14.57	17	9.02	2.80	0.33	0.20*	1.05*	HII	DS
1412	4503	Sa	12.12	17	10.53	5.95	-	-	-	NEL	LOI
1419	4506	18	13.64	17	9.66	3.44	0.57	0.35	-	HII	SDSS
1450	-	Sc	13.29	17	9.44	2.93	0.61	0.24*	0.42*	HII	DS
1508	4519	Sc	12.34	17	9.93	3.17	0.83	0.22*	1.17*	HII	DS
1516	4522	Sbc	12.73	17	9.85	3.12	0.46	0.33	0.22	HII	SDSS
1524	4523	Sd	13.51	17	9.49	-	0.75	0.14*	0.97*	HII	DS
1532	-	Sc	14.05	17	9.55	1.69	0.45	0.25	0.20	HII	SDSS
1540	4527	Sb	11.32	17	10.91	6.79	1.02	0.45*	-	LIN	Ho
1552	4531	Sa	12.58	17	10.22	3.00	-	2.69	-	Sey/LIN	MDS
1554	4532	Sm	12.30	17	9.90	2.92	0.26	0.12*	2.00*	HII	Ho
1555	4535	Sc	10.51	17	10.76	2.18	1.41	0.41	-	LIN/HII	LOI
1557	4533	Scd	14.53	17	9.12	2.83	0.34	0.22	0.88	HII	SDSS
1562	4536	Sc	11.01	17	10.71	6.96	1.61	0.50	-	LIN/HII	LOI
1569	-	Scd	15.00	17	8.42	3.16	0.54	0.12	1.71	HII	SDSS
1575	-	Sm	13.98	17	9.31	2.44	0.41	0.30*	0.08*	HII	DS
1581	-	Sm	14.55	17	8.74	2.77	-	0.05*	0.65*	HII	DS
1588	4540	Scd	12.81	17	10.05	2.25	0.49	0.34*	-	Sey	NED
1615	4548	Sb	10.98	17	10.91	4.34	1.46	22.14	-	LIN	Ho
1624	4544	Sc	13.89	17	9.68	2.77	0.51	0.31	0.42	HII	SDSS
1673	4567	Sc	12.08	17	10.41	2.73	-	0.39	-	HII	Ho
1675	-	Pec	14.47	17	8.96	2.87	0.37	0.17*	1.25*	HII	DS
1676	4568	Sc	11.70	17	10.71	4.27	-	0.34*	0.14*	HII	Ho
1678	-	Sd	13.70	17	8.81	2.91	0.54	0.10*	2.05*	HII	DS
1686	-	Sm	13.95	17	9.32	2.98	0.45	0.20*	1.51*	HII	DS
1690	4569	Sab	10.25	17	11.05	4.37	1.8	1.52	-	LIN	Ho
1696	4571	Sc	11.81	17	10.38	2.94	0.76	0.39*	-	HII	DS
1699	-	Sm	14.11	17	8.83	2.64	0.57	0.11*	4.85*	HII	DS
1725	-	Sm/BCD	14.51	17	8.97	2.92	0.34	0.14*	2.14*	HII	DS
1726	-	Sdm	14.54	17	8.64	2.73	-	-	1.18*	HII	DS
1727	4579	Sab	10.56	17	11.11	4.51	1.43	2.88	-	Sey	Ho
1730	4580	Sc	12.61	17	10.22	2.68	0.6	1.82	-	Sey/LIN	SDSS
1757	4584	Sa	13.60	17	9.54	3.53	0.63	0.34	0.11	HII	SDSS
1758	-	Sc	14.99	17	9.03	3.47	0.3	0.08*	1.31*	HII	DS
1760	4586	Sa	12.54	17	10.32	6.11	0.78	1.10	8.34	Sey	SDSS
1780	4591	Sb	13.70	17	9.63	3.01	0.43	0.39	0.20	HII	SDSS
1791	-	Sm/BCD	14.67	17	8.95	2.86	0.18	-	-	HII	DS
1811	4595	Sc	12.92	17	9.85	2.71	0.61	0.29*	0.60*	HII	DS
1813	4596	Sa	11.51	17	10.84	5.44	-	0.67	-	LIN	Ho
1859	4606	Sa	12.52	17	10.10	3.40	0.82	0.63*	-	Sey/LIN	DS
1868	4607	Scd	13.75	17	9.92	3.02	0.42	0.68	1.28	LIN	SDSS
1923	4630	Sbc	13.14	17	9.83	2.48	0.71	0.28	-	HII	LOI
1929	4633	Scd	13.77	17	9.46	3.14	0.49	0.20*	1.05*	HII	DS
1932	4634	Sc	13.19	17	9.99	3.08	0.15	0.40*	0.45*	HII	DS
1943	4639	Sb	12.19	17	10.26	3.54	0.94	1.18	-	Sey	Ho
1955	4641	S/BCD	14.32	17	9.36	4.17	1.04	0.24	0.31	HII	SDSS
1972	4647	Sc	12.03	17	10.51	3.06	-	0.28	-	HII	Ho
1987	4654	Sc	11.14	17	10.66	2.93	1.01	0.28	0.20	HII	Ho
1999	4659	Sa	13.08	17	10.04	6.03	-	-	-	NEL	DS
2023	-	Sc	13.86	17	9.17	3.09	0.36	0.15*	1.91*	HII	DS
2033	-	BCD	14.65	17	8.66	3.70	0.38	0.11*	1.48*	HII	DS
2058	4689	Sc	11.55	17	10.48	2.80	1.02	1.58	-	Sey/LIN	SDSS
2070	4698	Sa	11.53	17	10.75	5.78	1.22	4.84	-	Sey	Ho
13046	4045	Sa	13.50	17	10.25	5.05	0.97	0.89	1.28	LIN	SDSS
14063	4517	Sc	12.40	17	10.78	2.88	0.31	0.24*	0.85*	HII	DS
14110	4632	Sc	12.60	17	10.13	4.03	0.57	0.37	-	HII	LOI
15031	4771	Sc	13.30	17	10.14	3.73	0.5	1.30	-	Sey/LIN	SDSS
15032	4772	Sa	12.90	17	10.36	8.40	1.32	1.31*	-	LIN	Ho
15037	-	Scd	13.60	17	9.13	2.12	0.8	0.36	0.77	HII	SDSS
15049	4845	Sb	12.90	17	10.57	4.91	0.9	0.85	1.69	LIN	SDSS
15055	4904	Sc	13.20	17	10.04	2.70	0.84	0.32	-	HII	LOI
41041	4116	Scd	13.00	17	9.87	2.27	0.89	0.23*	0.51*	HII	DS
41042	4123	Sc	13.10	17	9.94	3.61	1.3	0.54	0.26	LIN/HII	Ho
43028	4688	Sc	14.50	17	9.52	2.41	0.7	-	-	LIN/HII	Ho
43034	4701	Sc	13.10	17	9.79	3.25	0.61	0.24*	0.88*	HII	DS
43041	4713	Sc	12.30	17	9.97	2.93	0.64	0.73	1.42	LIN/HII	Ho
43054	4765	Scd	13.00	17	9.43	2.75	0.56	0.11*	2.60*	HII	DS
43066	4799	Sd	14.40	17	9.76	4.59	0.63	1.70	-	Sey/LIN	SDSS
43071	4808	Sc	12.50	17	10.12	3.32	0.51	0.41*	0.68*	LIN/HII	DS
43093	4900	Sc	12.80	17	10.27	1.82	0.33	0.94	0.14	HII	SDSS
69036	4067	Sb	13.20	17	9.67	3.34	0.88	0.79	-	Sey/LIN	MDS
71060	4746	Sd	13.30	17	9.87	2.85	0.16	0.41	0.40	LIN/HII	SDSS
71068	4779	Sc	13.50	17	9.76	3.56	0.91	0.41	-	LIN/HII	LOI
71092	4866	Sa	11.90	17	10.54	6.28	-	-	-	LIN	Ho
100004	4651	Sc	11.30	17	10.52	2.98	0.82	1.13	-	LIN	Ho

Table 5: spectroscopic results

VCC/CGCG	NGC	TYPE	$m_{pg}$ mag (4)	$D$ Mpc (5)	$\log L_H$ $L_\odot$ (6)	$C_{31}(H)$ (7)	$Nuc(r)$ mag arcsec $^{-2}$ (8)	[NII]/H $\alpha$ (9)	[OIII]/H $\beta$ (10)	Spec Class (11)	Ref (12)
100015	4758	Scd	14.10	17	9.77	3.83	0.42	-	-	HII	DS
		not measured spectroscopically									
34	-	Sc	14.65	32	-	-	-	-	-	-	-
48	-	Sdm	14.30	32	9.28	2.70	0.53	-	-	-	-
99 <sup>†</sup>	-	Sa	14.81	32	9.56	3.02	-	-	-	-	-
275	-	Im	14.54	32	9.35	3.10	-	-	-	-	-
331	-	Pec	15.00	32	-	-	0.3	-	-	-	-
362 <sup>†</sup>	4266	Sa	14.51	32	10.46	3.60	-	-	-	-	-
434	4287	S..	14.65	23	9.49	3.93	0.44	-	-	-	-
449 <sup>†</sup>	4289	Sbc	14.34	17	9.72	5.70	0.7	-	-	-	-
514	-	Sc	14.70	23	-	-	-	-	-	-	-
517	-	Sab	14.90	17	9.42	-	0.43	-	-	-	-
531	-	Sa	15.00	17	8.79	-	0.33	-	-	-	-
567 <sup>†</sup>	-	Scd	14.36	23	9.16	2.65	0.62	-	-	-	-
697 <sup>†</sup>	-	Sc	14.17	23	9.66	3.02	0.73	-	-	-	-
768	-	Sc	14.91	17	8.90	3.16	0.32	-	-	-	-
826	-	Im	15.00	17	-	-	-	-	-	-	-
1017	-	Im	14.50	23	-	-	-	-	-	-	-
1114	-	Im	14.82	17	8.98	-	-	-	-	-	-
1435	-	Im	14.63	17	8.95	-	-	-	-	-	-
1442 <sup>†</sup>	-	Sd	14.82	17	-	-	0.31	-	-	-	-
1465	-	Im	15.00	17	-	-	-	-	-	-	-
1468	-	Im	15.00	17	-	-	0.19	-	-	-	-
1529	-	Sdm	14.63	17	-	-	0.07	-	-	-	-
1566	-	Sd	14.80	17	-	-	0.33	-	-	-	-
14062 <sup>†</sup>	-	Scd	14.10	17	9.63	2.87	0.57	-	-	-	-

Col 1: VCC or CGCG designation; Col 2: NGC name; Col 3: Hubble type from the VCC; Col 4: Photographic magnitude from the VCC; Col 5: Distance; Col 6: H-band luminosity; Col 7: H-band light concentration index; Col 8:  $r$ -band nuclearity parameter; Col 9: ratio of N[II]/H $\alpha$ . An asterisk indicates Drift-Scan spectra; Col 10: ratio of O[III]/H $\beta$ . An asterisk indicates Drift-Scan spectra; Col 11: Adopted spectral classification; Col 12: reference to the spectral classification: Ho=from Ho et al.(1997); SDSS: nuclear spectrum from the SDSS; DS=drift-scan spectrum; LOI=spectrum taken at Loiano; MDS= Modified drift-scan. <sup>†</sup> refers to the galaxies added in proofs (see footnote 2).

